Investigating the Role of Clasts on the Movement of Sand in Gravel Bed Rivers

A. (Thanos) N. Papanicolaou, F.ASCE[1]; Dimitrios C. Dermisis[2]; and Mohamed Elhakeem[3]

Abstract: The bed morphology of mountain rivers is characterized primarily by the presence of distinguishable isolated roughness elements, such boulders or clasts. The objective of this experimental study was to provide a unique insight into the role of an array of clasts in regulating sand movement over gravel beds for low relative submergence conditions, $H/d_c < 1$, and flow depth, H, to the diameter of the clast, d_c, a process that has not been studied thoroughly. To assess the role of clasts in controlling incoming sand movement, detailed flume experiments were conducted by placing 40 equally spaced clasts atop a well-packed glass bead bed for replicating the isolated roughness flow regime. The experiments were performed for moderate ($\sim 2.50\tau^*_{cr}$ where τ^*_{cr} is the critical dimensionless bed shear stress) and high ($\sim 5.50\tau^*_{cr}$) applied bed shear stress conditions, representative of gravel bed rivers. For comparison purposes, experiments were also repeated for nearly identical flow conditions but without the presence of clasts to discern the potential effects that clasts may have on sediment movement and hydraulics within the clast array region and also in the upstream section of the clast region where few observations exist. The experimental results revealed the formation of two distinguishable bed morphological features, namely a funnel shaped "sand ridge" upstream from the clast array region and small depositional "sand patches" around individual clasts. The sand patches were formed in the stoss region of the clasts, which contradicted previous observations of depositional patterns around clasts under high relative submergence conditions ($H/d_c > 1$) where, in this case, depositional patches were observed to have formed in the clast wake region. Furthermore, most of the incoming sand was found to be intercepted by the evolving sand ridge upstream from the clast array region with implications in the amount of sand entering the clast array region. The exiting bed-load rate was found to be reduced by a factor of ~5.0–20, depending on the prevailing flow conditions when experiments with and without clasts were compared under nearly identical flow conditions. The findings of this research, although limited to the isolated roughness regime, may have significant ramifications in stream restoration projects for the design of engineered riffle sections, which typically consist of an array of clasts installed to improve degraded waterways and aquatic habitat. **DOI: 10.1061/(ASCE)HY.1943-7900.0000381.**

CE Database subject headings: Submerging; River beds; Gravel; Deposition; Sand (hydraulic); Bed loads.

Author keywords: Clast array; Submergence; Sand bed; Gravel bed; Deposition; Sand ridge; Sand patches; Bed load; Resistance.

Introduction

The bed morphology of mountain rivers is characterized primarily by the presence of distinguishable isolated roughness elements, such boulders or clasts (e.g., Wohl 2000). The size of these clasts is comparable to the flow depth and believed to govern their surrounding hydrodynamics by triggering significant changes to the water surface profiles because of flow constriction and acceleration (e.g., Vallé and Pasternack 2006), causing the departure of the mean velocity profile from the logarithmic law attributable to flow separation and wake effects (e.g., Strom and Papanicolaou 2008), and affecting the transport and depositional patterns of incoming sediments attributable to the protection ("hiding factor") that is offered to the finer size incoming sediment (e.g., Rickenmann 1997).

Several studies have examined the flow structures around clasts (e.g., Boyer and Roy 1991; Shamloo et al. 2001; Papanicolaou and Kramer 2005; Polatel et al. 2005; Tritico and Hotchkiss 2005; Strom et al. 2007) under different packing densities or interchangeable spacing among clasts (e.g., Papanicolaou et al. 2001) and eluded that a key parameter that controls the flow characteristics around these elements is the ratio of the approach flow depth, H, to the diameter of the clast, d_c (the subscript c denotes clast). The ratio H/d_c is defined in the literature as "relative depth or submergence" and has been recorded to affect both the flow resistance of gravel bed streams and the depositional patterns and rates of sediment (e.g., Rickenmann 2001).

Fewer quantitative studies concern the role of the clasts in controlling incoming sediment movement (e.g., Strom et al. 2004; Papanicolaou and Kramer 2005; Yager et al. 2007). Most of these studies have focused solely on examining the sediment patterns around individual clasts for high relative submergence conditions (i.e., $H/d_c > 1$) and highlighted that immobile clasts usually become keystones for accumulation of incoming sediments in their wake region (e.g., Brayshaw 1984; Strom et al. 2004; Strom

[1]Professor and Donald E. Bently Faculty Fellow in Engineering, IIHR-Hydroscience and Engineering, Dept. of Civil and Environmental Engineering, Univ. of Iowa, 100 C. Maxwell Stanley Hydraulics Laboratory, Iowa City, IA 52242 (corresponding author). E-mail: apapanic@engineering.uiowa.edu

[2]Graduate Research Assistant, IIHR-Hydroscience and Engineering, Univ. of Iowa, 100 C. Maxwell Stanley Hydraulics Laboratory, Iowa City, IA 52242. E-mail: dimitrios-dermisis@uiowa.edu

[3]Assistant Research Engineer, IIHR-Hydroscience and Engineering, Univ. of Iowa, 100 C. Maxwell Stanley Hydraulics Laboratory, Iowa City, IA 52242; and Assistant Professor, Dept. of Civil Engineering, Collage of Engineering and Computer Science, Abu Dhabi Univ., Abu Dhabi, 59911, United Arab Emirates. E-mail: melhakee@engineering.uiowa.edu

Note. This manuscript was submitted on February 18, 2009; approved on December 14, 2010; published online on August 15, 2011. Discussion period open until February 1, 2012; separate discussions must be submitted for individual papers. This paper is part of the ***Journal of Hydraulic Engineering***, Vol. 137, No. 9, September 1, 2011. ©ASCE, ISSN 0733-9429/2011/9-871–883/$25.00.

J. Hydraul. Eng., 2011, 137(9): 871-883

and Papanicolaou 2008). Yet, limited information exists to date on sediment patterns around individual clasts under low relative submergence condition (i.e., $H/d_c < 1$) (e.g., Papanicolaou and Kramer 2005), which is considered to be representative of the average flow conditions in high-gradient gravel bed streams.

Furthermore, very few studies have examined the collective role of an array of clasts (referred to hereafter as "clast array region") on bed morphology and sediment movement under $H/d_c < 1$ (e.g., Papanicolaou and Kramer 2005; Yager et al. 2007). Most of these studies gloss over the role of the clast array region on the hydraulics (e.g., backwater effects), sediment movement, and bed morphological features in the upstream section of the clast array region. The potential ramifications on sediment movement and hydraulics attributable to morphological changes occurring within the clast array region and also in the upstream section of the clast region remain unknown.

The overarching objective of this experimental study is to provide a unique insight into the role of an array of clasts in regulating sand movement in gravel bed streams for low relative submergence conditions, a process that has not been studied thoroughly (e.g., Parker 2008). Understanding the role of a clast array region on sand movement (i.e., bed load) requires knowledge of the depositional patterns of the incoming sand and the flow characteristics around these elements and in the upstream section. Thus, the following tasks were undertaken: (1) the determination of the incipient motion condition of the sand particles to establish a baseline condition for the bed-load observation tests; (2) the aerial description of the sand depositional patterns upstream of the clast array region and around the individual clasts; (3) the investigation of the effects of clasts on bed-load rates; (4) the performance of a mass balance analysis to determine the percentage of the incoming sand that enters and exits the test section; (5) the examination of the flow characteristics in the vicinity of the clasts and the potential role of flow on the depositional patterns observed around the clasts; and (6) the determination of the added resistance provided by the bed morphological features and the clasts to the flow.

Experimental Setup and Procedures

Facilities and Instrumentation

The experiments were conducted in a water-recirculating tilting flume (see Fig. 1), with a working section length of 21.6 m, a width of 0.90 m, and a depth of 0.50 m, located in the hydraulics laboratory of the IIHR-Hydroscience and Engineering at the University of Iowa (http://www.iihr.uiowa.edu/facilities/rsflume/flume2.html). The flume had clear sides (i.e., acrylic walls) to facilitate viewing and video recording. The gradient of the flume was adjusted by the operation of a mechanical jack screw with a precision of 0.01%. A closed operating system with a centrifugal pump of maximum discharge of 50 L/s was used to recirculate the water. The flow rate was measured by using an electromagnetic digital flowmeter with an accuracy of −0.25%. The flume included two mobile carriages. The first carriage was equipped with five point gages that can provide measurements to the nearest millimeter, equally spaced at a distance of 0.15 m across the transverse direction of the flume, for mapping the bed and water surface elevations [Fig. 1(a)]. To obtain the bathymetry of the bed and the flow depth at different cross sections, the carriage was manually moved along the longitudinal direction of the flume. The second carriage was used for monitoring and visualization by mounting a video camera [Fig. 1(b)]. The bed-load rate was measured by using a sediment trap located at the downstream end of the flume.

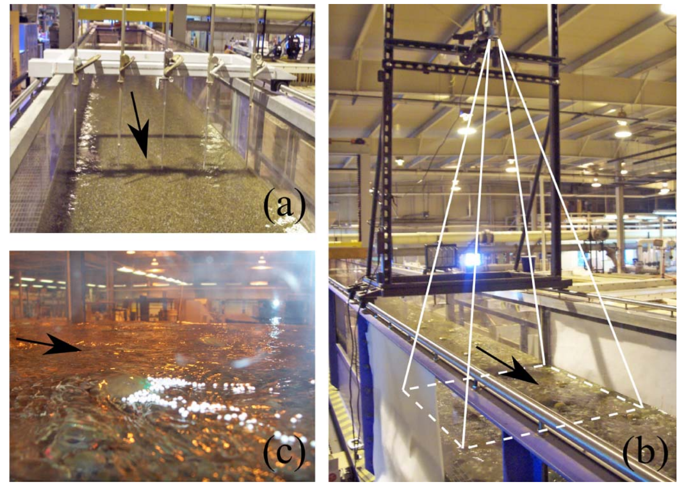

Fig. 1. (a) Flume carriage equipped with five point gages to determine bed morphology and water surface profile; (b) second flume carriage equipped with a video camera for performing LSPIV measurements; (c) polystyrene foam particles used during LSPIV measurements; arrows indicate flow direction

Test Sections

The flume consisted of the following three sections (Fig. 2): (1) the upstream "sand bed section," which served as a sand feeding section; (2) the middle "glass bead bed section," which constituted the primary test section; and (3) the downstream "exit section," which included the sediment trap and the tailgate.

The sand bed section (9.6 m in length) consisted of an 8.0 cm thick layer of near uniform natural sand (geometric standard deviation of $\sigma_g = 1.19$), with a mean particle size of $d_{50} \approx 1.9$ mm and a specific gravity of $SG = 2.50$. Uniform sand was chosen to eliminate factors such as hiding-exposure and sorting on the transport of sand.

The glass bead bed section (5.0 m in length), representing the gravel bed, was comprised of five layers (8.0 cm thick) of immobile, well-packed, uniform spheres (glass beads). The glass beads had a diameter of $d \approx 19$ mm, a specific gravity of $SG = 2.58$, and an average porosity of $n_p = 0.24$. The well-packed bed provided a uniform roughness surface and minimized the effects of protrusion. Forty (40) isolated, immobile, spherical particles with a diameter $d_c = 55$ mm, representing the clasts, were placed atop the glass bead bed, forming the clast array region (see Fig. 2). The spacing among the clasts was chosen to be six times their diameter, d_c. This spacing corresponded to an isolated roughness flow regime having a 2% packing density (Morris 1955).

The exit section (4.0 m in length) consisted of a flat plywood bed and included a sediment trap and collector for bed-load measurements and a tailgate at the downstream end of this section for controlling the flow depth (Fig. 2). Once the sand was collected from the sediment trap, the bed-load rate, g_b (kg/m/h), was determined.

Experimental Procedures

DIMOS Experiments

A series of experiments was conducted first for determining the incipient motion of sand particles (DIMOS experiments) without the presence of clasts to (1) determine when the commencement of sand movement occurred; and (2) establish the baseline flow conditions for the remaining experiments (described in the next section) focused on the effects of an array of clasts on sand

J. Hydraul. Eng., 2011, 137(9): 871-883

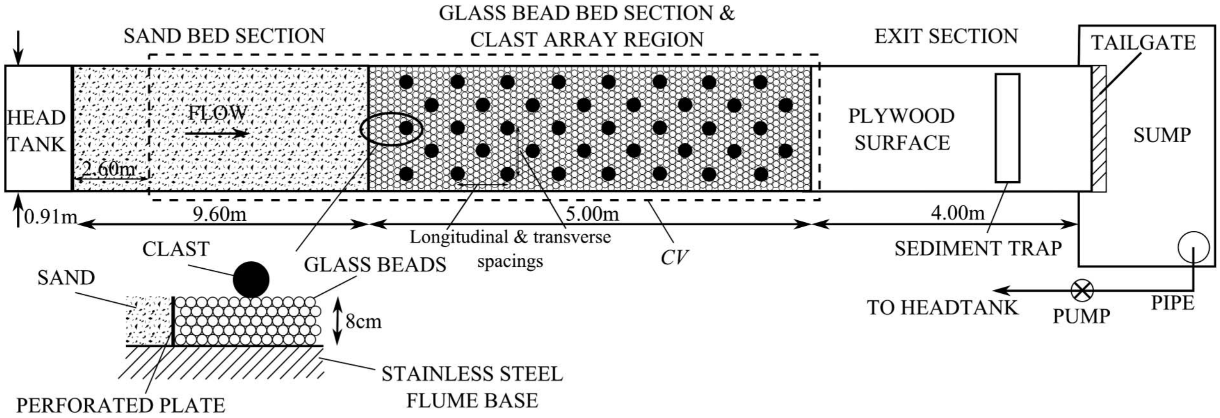

Fig. 2. Plan view of flume with test sections (not to scale); side view of bed detail consisting of 5 layers of glass beads

movement over gravel beds. The incipient motion criterion for the individual sand particles was determined by using the probability of entrainment concept by Papanicolaou et al. (2002). This concept accounts for the near-bed turbulent effects (cycle of turbulent bursts) and frequency of their occurrence; thus, it does not overestimate the critical flow conditions under which the commencement of sediment motion occurs (Papanicolaou et al. 2002). The incipient condition of the sand particles was considered for a 1.0% probability of entrainment; that is, during a bursting cycle, one of 100 particles is transported by near-bed turbulence.

To perform DIMOS experiments, the 8.0 cm sand bed section was leveled and stabilized by using the "freezing" technique, described by Benson et al. (2001), to ensure no changes in the bed roughness. A video camera (20× optical zoom) was positioned vertically over the flume to provide a plan view of the stabilized section, and mobile, colored sand particles ($d_{50} \approx 1.9$ mm) were placed atop the stabilized bed far enough from one another to minimize their interaction (Papanicolaou et al. 1999). The flow depth, H, was gradually increased by adjusting the flow discharge for a given slope, S, maintaining uniform flow conditions. The particle movement was continuously recorded, and the video files were processed by using Image J software to calculate the percentage of particle movement for the tested flow depths, H. The critical flow depth, H_{cr}, corresponding to a 1.0% particle entrainment was used to determine the dimensionless critical bed shear stress, τ^*_{cr}, defined as

$$\tau^*_{cr} = \frac{H_{cr}S}{(SG-1)d_{50}} \tag{1}$$

where SG = specific gravity of sand. The τ^*_{cr} was determined to be 0.022 on the basis of the outcomes from 10 experimental runs. After the completion of the 10 experiments, the stabilized sand bed was replaced with a new 8.0-cm-thick sand bed layer for the sequent experiments.

Sand Movement over Gravel with Clasts and Sand Movement over Gravel Experiments

Two experimental scenarios were considered to investigate the role of the array of clasts on the movement of sand over gravel beds: (1) sand movement over gravel with clasts (SMOGC) experiments were performed with the presence of clasts; and (2) sand movement over gravel (SMOG) experiments were performed without the presence of clasts. SMOGC and SMOG experiments were conducted under nearly identical bed shear stresses and flow discharges to provide a comparison of conditions with and without clasts for sand movement and associated sand features. The flow conditions for these experiments were defined on the basis of the dimensionless critical bed shear stress, τ^*_{cr} (i.e., reference stress), determined from the DIMOS experiments. Specifically, the dimensionless applied bed shear stress, τ^*, was chosen to be ~$2.50\tau^*_{cr}$ (≈ 0.056) for moderate bed shear stress (i.e., SMOGC-1 and SMOG-1 experiments) and ~$5.50\tau^*_{cr}$ (≈ 0.120) for high bed shear stress conditions (i.e., SMOGC-2 and SMOG-2 experiments). These values were within the range of observed dimensionless bed shear stress values for gravel bed rivers (e.g., Mueller et al. 2005). SMOGC experiments were designed to represent the low relative submergence conditions of $H/d_c = 0.8$, or, equivalently, a flow depth of $H = 0.044$ m measured over the sand bed section (i.e., well upstream of the clast array region), by adjusting the flow discharge, Q, and the tailgate at the beginning of the experiments. At the beginning of the experiments, the procedure of adjusting the flow conditions in the flume lasted approximately 5 min or less. During this period, an insignificant movement of sand was observed.

The procedure used for the SMOGC-1 and SMOGC-2 experiments included the placement of 40 clasts atop the glass bead bed and setting the slope, S, of the flume equal to the value derived from the following equation:

$$S = \frac{\tau^*(SG-1)d_{50}}{H} \tag{2}$$

for the selected τ^* and flow depth, H (SG and d_{50} are the specific gravity and mean particle size of the sand, respectively). During the SMOGC experiments, the net volume of sand that was eroded or deposited with time in the sand bed section was determined by measuring the bathymetry of the sand bed by using the five point gages described earlier. The mapping interval for measuring the bathymetry of the sand bed was varied between two times per day (SMOGC-1) up to every 20 min (SMOGC-2). These intervals were determined to ensure insignificant changes in the sand bed bathymetry during the bed scanning process. The same technique was used to determine the net volumes of sand that eroded or deposited within the clast array region. In this case, however, the positions of the gages were readjusted by placing the gages 0.02 m apart, across the transverse direction of the flume, to capture the dimensions of the sand deposits around the clasts. The duration for performing a full scan of the bed morphological features was approximately 10–20 min. The volume of sand that infiltrated the porous structure of the glass bead bed was measured only at the termination of each experiment by excavating each layer of glass beads and sweeping: (1) the sand particles that had adhered to the bead surface; and (2) the sand found within the porous structure. Finally, the volume of sand that exited the clast array region was determined by drying and weighting the sand collected in

J. Hydraul. Eng., 2011, 137(9): 871-883

Table 1. Hydraulic Parameters of the Four Experiments

Variable[a] Experiment	τ^*	H/d_c	H (m)	b/H	S	Q (m^3/s)	U_{bulk} (m/s)	F	R	R_o
SMOGC-1	0.056	0.8	0.044	20	0.0036	0.014	0.35	0.54	62,200	12.6
SMOG-1	0.056	—	0.040	23	0.0040	0.014	0.39	0.62	62,200	12.6
SMOGC-2	0.120	0.8	0.044	20	0.0078	0.017	0.43	0.65	75,500	8.6
SMOG-2	0.120	—	0.039	23	0.0088	0.017	0.48	0.78	75,500	8.6

[a]The variables are: (1) applied dimensionless bed shear stress, τ^*, defined as $\tau^* = \tau/[\rho g(SG-1)d_{50}]$ where τ = applied bed shear stress; g = gravitational acceleration; ρ = water density; and SG and d_{50} = specific gravity and the mean particle size of the sand, respectively; (2) relative submergence, H/d_c; (3) flow depth, H (datum of $z = 0$ was considered to be the top of the glass beads); (4) width to depth ratio, b/H, where b = flume width; (5) slope of the bed, S, derived from the specified dimensionless applied bed shear stress, τ^*, and flow depth, H; (6) flow discharge, Q; (7) bulk velocity, U_{bulk}, defined as $U_{\text{bulk}} = Q/A$ where A = cross-sectional flow area; (8) Froude number, F, defined as $\mathsf{F} = U_{\text{bulk}}/\sqrt{gH}$; (9) Reynolds number, R, defined as $\mathsf{R} = 4HU_{\text{bulk}}/\nu$ where ν = kinematic viscosity of the water equal to 10^{-6} m^2/s; and (10) Rouse number, R_o, defined as $R_o = \omega/\kappa\sqrt{\tau/\rho}$ where ω = fall velocity of the sand particles determined on the basis of the equation developed by Dietrich (1982) and $\kappa \sim 0.4$ denotes the von Kármán constant.

the sediment trap during the experiments at regular time intervals, varying between ~12 h and ~1 min, depending on the duration of the experiments; the duration of the experiments varied depending on the flow conditions and the presence or absence of clasts. A moderate applied bed shear stress ($\tau^* \approx 2.50\tau^*_{cr}$) with the presence of clasts delayed the movement of sand particles (i.e., SMOGC-1 experiment lasted ~825 h), whereas a higher in magnitude bed shear stress ($\tau^* \approx 5.50\tau^*_{cr}$) without clasts enhanced the bed-load transport (i.e., SMOG-2 experiment lasted ~1.0 h). A similar experimental procedure was followed for SMOG-1 and SMOG-2 experiments, but no clasts were placed over the glass bead bed.

A summary of the hydraulic parameters for the SMOGC-1, SMOG-1, SMOGC-2, and SMOG-2 experiments is provided in Table 1. The values of the flow depth, H, and bed slope, S, (and other variables reported in Table 1 that were determined indirectly from the H and S values) in SMOGC experiments correspond to the beginning time of the experiments (i.e., initial conditions). In the early stages of the SMOGC experiments, the bed morphological features (discussed subsequently) were not present along the three flume sections defined in Fig. 2. Furthermore, the flow depth, H, reported in Table 1 was measured well upstream of the clast array region; however, H varied along the longitudinal direction of the flume during the experiments because of erosion or deposition occurring at the different flume sections. More information about the values of the flow depth, H, along the longitudinal direction of the flume for different time periods can be found in Fig. 3(b). Lastly, the Rouse number, R_o, in Table 1 was chosen to be greater than 5 to ensure that the sand was moving as bed load.

Flow Velocity Measurements

One hindrance in the performance of the velocity measurements was the shallow flow depth conditions ascribed to the low relative submergence. Velocity instruments such as acoustic Doppler velocimeters (ADVs) require a minimum water depth of approximately 5–10 cm that hampers their use in shallow water flows (e.g., Meselhe et al. 2004). Detailed flow measurements with a regular particle image velocimetry (PIV) system were feasible in this research but required an elaborate experimental design (i.e., bed modifications to facilitate laser access through the bed). In addition, as the field of view in the PIV recordings was limited to ~1 clast size diameter and the influence of the clasts to the flow in the downstream direction extended five to six times the clast size diameter, the regular PIV required "splicing" to merge a sequential series of PIV recordings in the streamwise direction, which was laborious (Papanicolaou and Kramer 2005). A technique that was deemed suitable for this study is large scale particle image velocimetry (LSPIV). LSPIV is based on the conventional PIV principles; more information about this relatively new technique can be found in Muste et al. (2004), Fox and Patrick (2008) and Hauet et al. (2008). The LSPIV provided two-dimensional (2D) free-surface velocity measurements for a large portion of the clast array region (i.e., length = 0.9 m and width = 0.75 m), thus presenting useful information about the flow patterns at a geometric scale that was

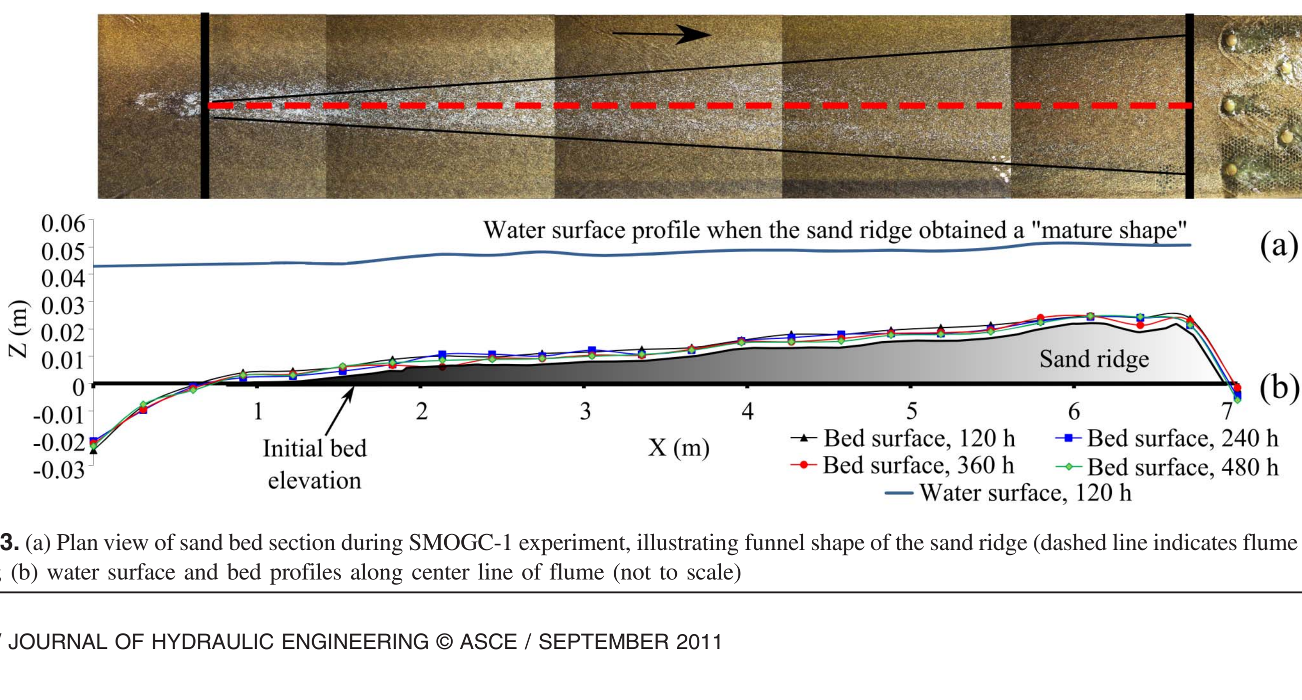

Fig. 3. (a) Plan view of sand bed section during SMOGC-1 experiment, illustrating funnel shape of the sand ridge (dashed line indicates flume center line); (b) water surface and bed profiles along center line of flume (not to scale)

J. Hydraul. Eng., 2011, 137(9): 871-883

comparable to the clast size and the whole clast array region. In this study, the motion of flow was traced by seeding the flow with tracer particles lighter than the density of water [i.e., 2 mm polystyrene foam expanded polystyrene beads, as shown in Fig. 1(c)]. A digital video camera, operating at a frequency of 30 Hz, was mounted in the flume carriage and captured the movement of the polystyrene foam particles for approximately 1 min, producing 1,800 sequential images. Instantaneous $u(t)$ and $v(t)$ velocity measurements of the longitudinal and transverse directions, respectively, were obtained from measuring the displacement of the particles. The velocity information was analyzed by using the cross-correlation method through a commercial particle image velocimetry program (LSPIV 2.0) (Kim 2006). The errors associated with this technique were less than 1.5% (Muste et al. 2004). For comparison purposes, LSPIV measurements were recorded for the SMOGC-1 experiment (1) with; and (2) without the presence of the bed morphological features along the flume sections described in the "Results" section. To perform the LSPIV measurements for the second case, the SMOGC-1 experiment was repeated under the same flow conditions as those presented in Table 1 by freezing the sand bed, similar to the technique used for the DIMOS experiments; thus, preventing the formation of the bed morphological features.

Results

The results of DIMOS and SMOGC/SMOG experiments are organized as follows: First, the incipient motion condition for the movement of sand particles and the corresponding critical bed shear stress are presented (DIMOS experiments). Second, a detailed description of the bed morphological features upstream and within the clast array region for the SMOGC and SMOG experiments is provided. Third, the time series of the measured bed-load rates are analyzed for SMOGC and SMOG experiments. Fourth, the mass balance analysis in a flume bed area, including the sand bed section and the clast array region (see dashed region in Fig. 2, which is defined hereafter as the control volume CV) to determine the percentage of the incoming sand that exited the CV and the percentage that was trapped within the CV, forming the unique bed morphological features is described. Fifth, an analysis of the free-surface velocity measurements and calculation of the vorticity around the clasts for the SMOGC-1 experiment is presented. Finally, the aforementioned velocity measurements to determine the added resistance provided by the bed morphological features and the clasts to the flow are presented.

Dimensionless Critical Bed Shear Stress

The analysis of the DIMOS experiments yielded $\tau_{cr}^* = 0.022$ for a 1.0% probability of entrainment, which is a more conservative value than the one obtained from the traditional Shields diagram. Nevertheless, the determined dimensionless critical stress compared satisfactorily to the value reported by Keshavarzy and Ball (1999), who used a similar technique of image analysis and processing for detecting the commencement of sand particles movement for a mean particle diameter of $d_{50} = 2$ mm, and $\tau_{cr}^* = 0.022$ for a 4.0% probability of entrainment. The small difference between the probability of entrainment of this study and the work by Keshavarzy and Ball (1999) was attributed to the fact that Keshavarzy and Ball (1999) investigated the incipient motion condition of sand particles moving atop a mobile bed, whereas the movement of particles for DIMOS experiments was observed atop a stabilized sand bed layer.

Bed Morphological Features

During the SMOGC experiments, two distinct, ubiquitous bed morphological features were formed: (1) a funnel shaped (V-shape), sand depositional bed feature located upstream of the clast array region, namely a "sand ridge" [Figs. 3(a) and 3(b)]; and (2) depositional "sand patches" around the individual clasts [Figs. 4(a) and 4(b)]. The formation of the sand ridge preceded the formation of the sand depositional patches. For the SMOGC-1 experiment, the sand ridge formed and obtained its "mature shape" (i.e., no further growth in space with time) within the 5 five days (120 h) of the experiment whereas the depositional patches mostly formed within a 15–20 day (360–480 h) period following the formation of the ridge. During the progression of the SMOGC-1 experiment, sand particles also infiltrated the porous structure of the glass bead bed. A similar sequence of sand ridge and depositional patch development and sand infiltration was observed for the SMOGC-2 experiment. In that case, because of the higher applied bed shear stress conditions (see Table 1), the time scales for the formation of the bed features were considerably shorter; the sand ridge formed within the first 20 min (0.3 h) of the experiment, and the depositional patches formed within 50–60 min (0.8–1 h) after the formation of the ridge.

The cause for the formation of the sand ridge in the SMOGC experiments was considered to be the increased resistance exerted by the clast array region to the flow. (Calculations of the added resistance for the SMOGC-1 experiment are provided in the "Flow Resistance" section.) Similarly, the formation of the depositional patches around the clasts was considered an outcome of the interaction between the flow and the individual clasts. These interactions differ for the two SMOGC experiments, and their effects are reflected by the different depositional patterns found within the clast array region [see Figs. 4(a) and 4(b)].

The formation of the sand ridge and sand patches over the sand and glass bead bed sections, respectively, altered the flow conditions in these sections. Flow within the sand bed section was unsteady and nonuniform because of the growth of the sand ridge with time and longitudinal distance. For example, for the SMOGC-1 experiment, at the point at which the sand ridge obtained its mature shape, flow in the sand bed section remained gradually varied [Fig. 3(b)]. Nonuniform flow conditions were present between the entrance of the sand ridge ($H = 0.038$ m) and the crest of the ridge ($H = 0.026$ m). This nonuniformity prevailed within the sand ridge section because of the control exerted downstream by the array of the 40 clasts. The 40 clasts created backwater effects attributable to flow constriction. Flow in the glass bead bed section was accelerated locally because of the lateral constriction of the clasts. As the experiment progressed, the formation of the small sand patches around the individual clasts caused additional lateral constriction effects to the flow. An analysis of the flow features in the vicinity of the clasts complemented with the depositional pattern observations for SMOGC-1 experiment is presented in the "Flow Measurements around the Clasts" section.

Contrary to the SMOGC experiments, during the SMOG experiments, the bed morphological features were not recorded because of the absence of the clast array region. A comparison of the SMOGC and SMOG experiments suggest that the array of clasts created favorable conditions for sand deposition upstream and within the clast array region, leading to the formation of distinguished bed morphological features; that is, the sand ridge and patches. The formation of these bed features has not been reported before in the literature, and their geometric characteristics are described in detail subsequently.

J. Hydraul. Eng., 2011, 137(9): 871-883

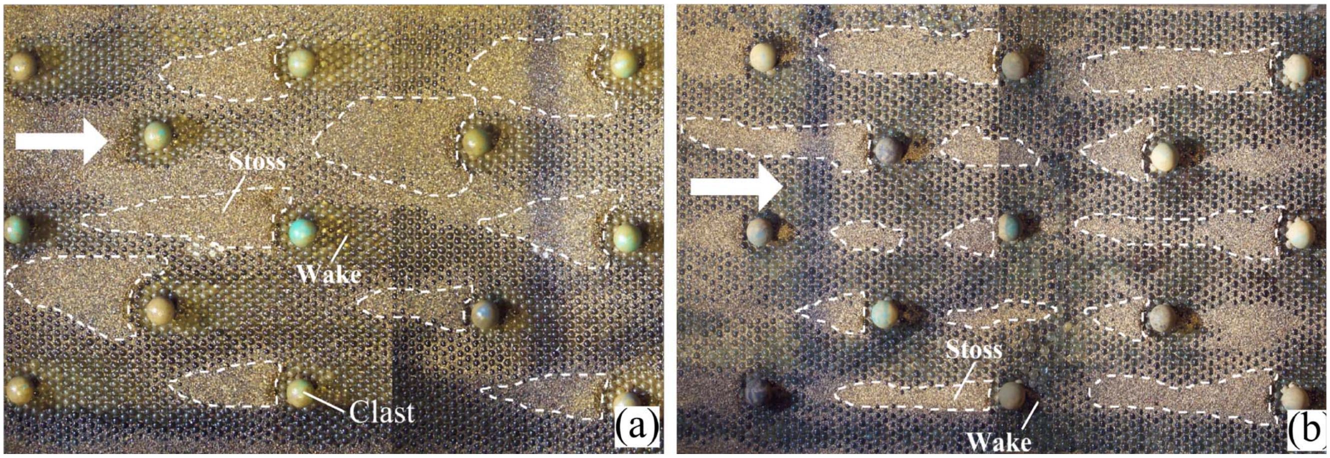

Fig. 4. Plan view of glass bead bed section at the end of SMOGC-1 and SMOGC-2 experiments, respectively (dashed lines indicate sand patches)

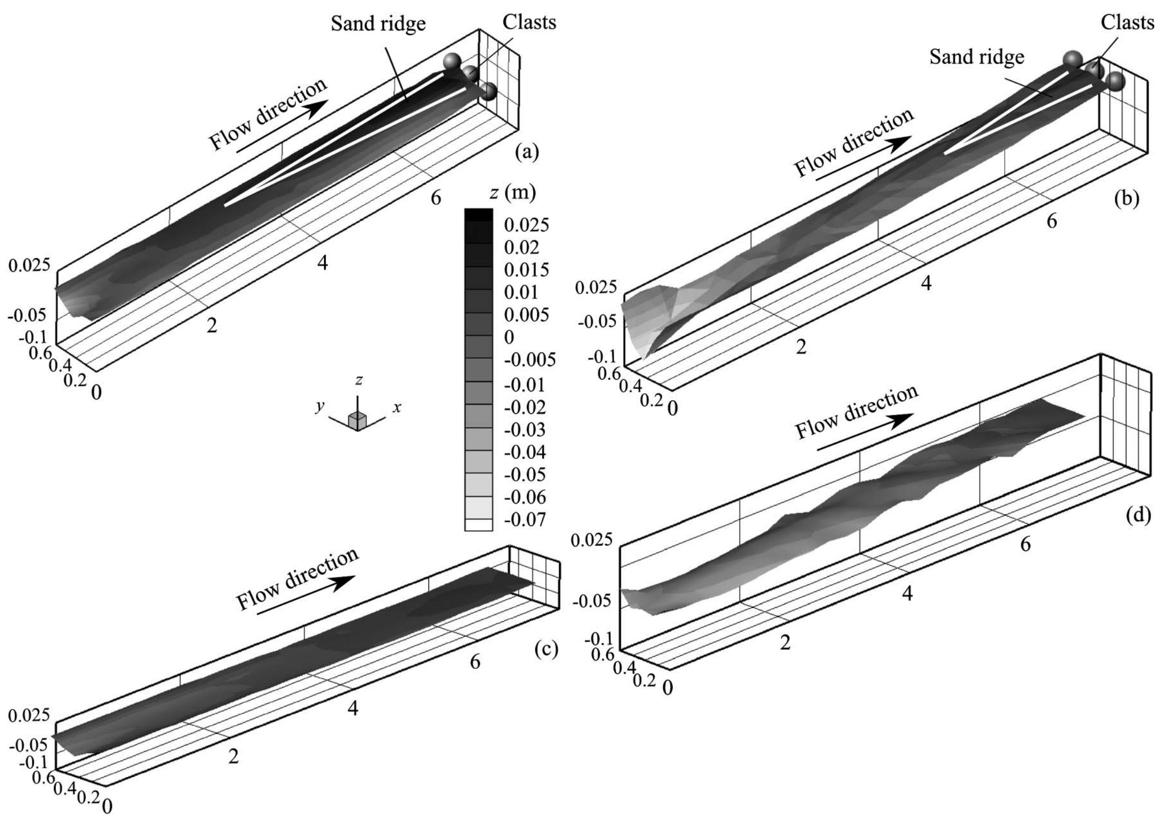

Fig. 5. 3D representation (not to scale) of bed morphology in sand bed section for case of: (a) SMOGC-1; (b) SMOGC-2; (c) SMOG-1; and (d) SMOG-2 experiments; elevation $z = 0$ corresponds to the initial level of the flat bed

Morphology of the Sand Bed Section Upstream of the Clast Array Region

A 3D representation of the sand ridges, which exhibited a convex funnel shape, upon the completion of the SMOGC-1 and SMOGC-2 experiments, is shown in Figs. 5(a) and 5(b), respectively. The 3D representations were constructed from bed elevation measurements by using the five point gauges [Fig. 1(a)] in 24 cross sections spaced 0.30 m apart, covering a distance of ~7.0 m upstream of the clast array region. The first ~2.6 m downstream of the flume entrance, not shown in the 3D representations, refer to the region in which significant erosion occurred and supplied sand particles to the downstream sections. The sand ridge in SMOGC-1 experiment [Fig. 5(a)] attained a length of ~5.5 m and a width and height that increased along the longitudinal direction of the flume from 0 to ~0.5 m and from 0 to ~0.02 m, respectively. The maximum height, 0.02 m, and width, 0.5 m, of the sand ridge were recorded immediately upstream of the clasts, where a vertical depositional front was developed [see also Fig. 3(b)]. In the SMOGC-2 experiment [Fig. 5(b)], the presence of higher bed shear stress reduced the length and maximum height of the sand ridge to ~2 m and ~0.007 m, respectively; however, similar geometric characteristics were observed. Figs. 5(c) and 5(d) provide the 3D bed morphology plots for the SMOG experiments and show that erosion occurred in the sand bed section, as expected.

J. Hydraul. Eng., 2011, 137(9): 871-883

Distribution of Sand Particles within the Clast Array Region

Plan views of the depositional sand patches for the SMOGC-1 and SMOGC-2 experiments are illustrated in Figs. 4(a) and 4(b). The formation of the patches mostly occurred in the stoss region of the individual clasts, where elongated V-shape ridges, with similar geometric characteristics to those of the large sand ridge, developed. However, a careful comparison of Figs. 4(a) and 4(b) reveals that the spatial distribution of the depositional patterns over the clast array region is distinctly different. For the SMOGC-1 experiment, the distribution of the sand patches corresponded to a "chessboard" morphology characterized by short and wide bed features with an average length of 0.17 m and width 0.12 m. A similar pattern of this morphology was noted by Bunte and Poesen (1993), although the deposition in their case occurred in the wake of the rocks. On the contrary, for the SMOGC-2 experiment, the depositional patches were found to be "in-line" with the clast rows along the longitudinal direction and were characterized by elongated and narrow bed features with an average length of 0.25 m and width 0.07 m. In the SMOGC-2 experiment, "straight-line corridors" that were free of sand depositional patches developed between two adjacent rows of clasts in the flume longitudinal direction. Instead, the arrangement of the patches in a chessboard morphology in the SMOGC-1 experiment resulted in "zig-zag shaped corridors." The differences in the spatial distribution of the sand patches were attributed to the different flow conditions (i.e., τ^*) and the mechanisms of flow-clast interactions between the two experiments. The association of the flow mechanisms with the sand patches for the two SMOGC experiments is further examined in a subsequent section.

A notable difference between the SMOGC experiments and others reported in the literature that are focused on the role of clasts in sediment depositional patterns, is the location of the depositional patches around the clasts. In the present study, the patches form in the stoss region of the clasts, whereas most of the available experimental studies (e.g., Brayshaw 1984; Bunte and Poesen 1993; Strom et al. 2004) reported the accumulation of sediment in the wake region of the clasts. The reversal behavior in the location of the depositional patches around the clasts has not been examined thoroughly in the literature because most available studies have focused on depositional patches under high relative submergence conditions, for which particle deposition occurred in the wake area behind the clasts, extending to the flow reattachment point (e.g., Strom et al. 2004). It was hypothesized that the location of depositional patches in the stoss of the clasts for low relative submergence relates to the differences in flow mechanisms for the two submergences. A discussion of the implications that this finding may have on stream restoration designs is provided.

Bed-Load Rate Time Series

The time series of the bed-load rates, g_b (Kg/m/h), for the SMOGC and SMOG experiments are presented in Figs. 6 and 7, respectively. These figures provide the measured bed-load rates (shown in symbols) and the predicted bed-load rates (solid line) obtained by an established bed-load formula (Misri et al. 1984) applicable to the present experimental conditions. The square symbols in Fig. 6 refer to the sand bed section and represent changes in the volume of the sand ridge recorded during the "variable rate" (i.e., bed-load rate changes with time) period of the experiments. The triangle symbols refer to the bed-load rate determined from the sand collected in the sediment trap at the exit section of the flume. The overall reduction in the bed-load rate with time was attributed to the added resistance by the sand ridge and sand patches to the flow. For the SMOGC-1 experiment, the sharp decay in bed-load rate [Fig. 6(a)], compared to the gradual decay for the SMOGC-2 experiment [Fig. 6(b)] was attributed to the larger volume of the

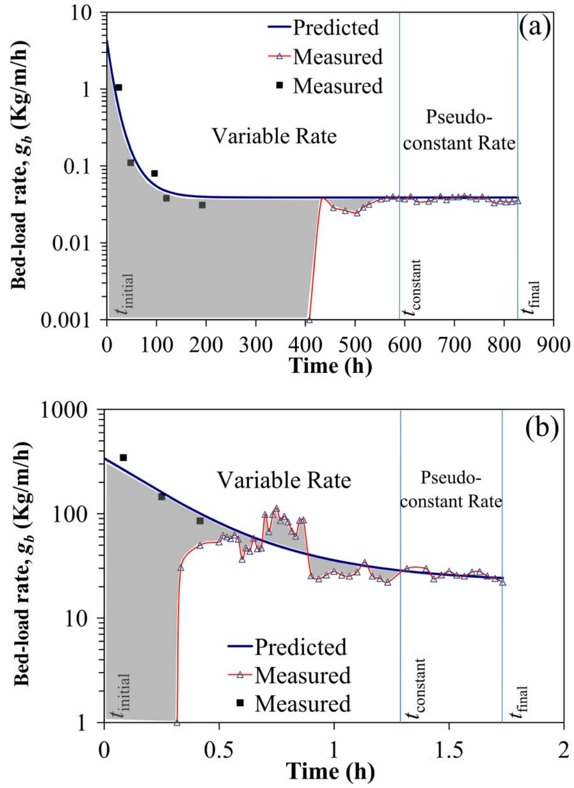

Fig. 6. Time series of the bed-load rates: (a) SMOGC-1; (b) SMOGC-2

sand ridge in the former case [see Figs. 5(a) and 5(b)]. Clearly, the period of 120 h in which the sharp decay occurs in Fig. 6(a) coincides with the period that the ridge obtained its mature shape and confirms the visual observations reported in the "Bed Morphological Features" section for the SMOGC-1 experiment. For the period between 120 and 460 h, the reduction in the bed-load rate is smaller than the first 120 h, and the fluctuations shown around the average bed-load rate are mostly attributed to the effects of sand patches and the influx of sand in the porous structure of the glass bead bed. The shaded areas underneath the measured/predicted curve in Figs. 6(a) and 6(b) represent (1) the net amount of sand that led to the formation of the two bed morphological features; and (2) the amount of sand intruded into the porous bed. The first 20 min in Fig. 6(b) coincide with the formation of the sand ridge in the SMOGC-2 experiment, whereas the remaining time period illustrates the effects of the sand patches and sand intrusion into the porous bed structure.

The SMOGC-1 and SMOGC-2 experiments were terminated at 830 h and 1.7 h (see Fig. 6), respectively, after the bed morphological features obtained a mature shape [sand ridge at 120 h (SMOGC-1) and 0.3 h (SMOGC-2); sand patches at 360–480 h (SMOGC-1) and 0.8–1 h (SMOGC-2)] and the bed-load rates at the flume exit reached a "pseudoconstant rate" [at 580 h (SMOGC-1) and 1.3 h (SMOGC-2)]. The pseudoconstant rate was reached before the supply of sand from the upstream sand bed section became limited. Subsequently, the geometric characteristics of the formed bed features were not influenced by limited sediment supply conditions, which was the case otherwise (e.g., Kleinhans et al. 2002; Tuijnder et al. 2009).

The bed-load rate time series for the SMOG-1 and SMOG-2 experiments in Figs. 7(a) and 7(b), respectively, reveal a relatively constant average bed-load rate because of the absence of the clast array region. By comparing the pseudoconstant and average bed-load rates for the SMOGC and SMOG experiments, respectively,

J. Hydraul. Eng., 2011, 137(9): 871-883

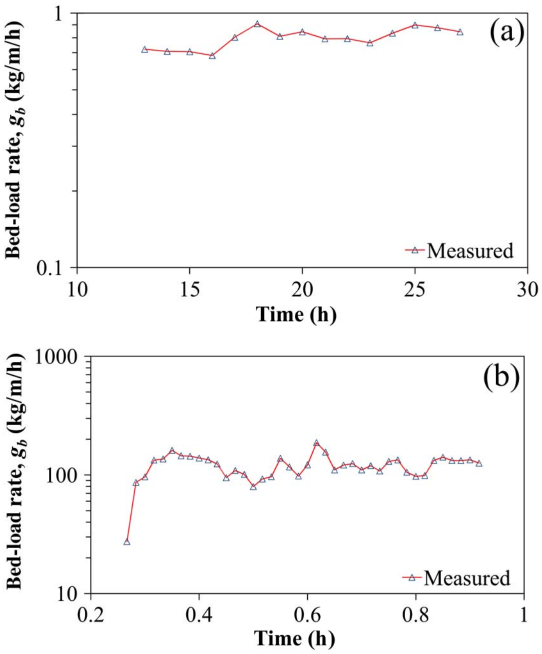

Fig. 7. Time series of the bed-load rates: (a) SMOG-1; (b) SMOG-2

one can surmise that for moderate bed shear stress conditions (i.e., $\sim 2.50\tau^*_{cr}$), the presence of clasts reduced the bed-load rate, on average, by a factor of ~20, whereas for higher bed shear stress conditions (i.e., $\sim 5.50\tau^*_{cr}$) by a factor of ~5.0.

To use the Misri et al. (1984) formula for predicting the bed-load rate in the section upstream of the sand ridge and in the variable and pseudoconstant rate periods of the experiments, the expression of the dimensionless bed shear stress equation was modified to account for the changes in the average bed slope along the flume attributable to the formation of the bed morphological features. The modified bed shear stress equation is as follows:

$$\tau^* = \frac{HS(t)}{(SG - 1)d_{50}} \tag{3}$$

where $S(t) = S_{\text{constant}} + (S_{\text{initial}} - S_{\text{constant}})e^{-kt}$ and k (L/s) = decay constant of the bed gradient or, equivalently, the rate at which the incoming sand accumulates in the sand ridge and patches around the clasts. For estimating k, first $S_{\text{initial}} = S$ where the initial bed slope values, S, are provided in Column 6 of Table 1. The final bed slope, S_{constant}, was then measured with the point gauges for the SMOGC experiments once a pseudoconstant bed-load rate was attained at t_{constant}. For SMOGC-1, the $S_{\text{constant}} = 0.0020$ and was attained at $t_{\text{constant}} = 580$ h, and for SMOGC-2, $S_{\text{constant}} = 0.0045$ and was reached at $t_{\text{constant}} = 1.3$ h.

By substituting Eq. (3) into the Misri et al. (1984) formula, the predicted bed-load rate, g_b (shown with solid line in Fig. 6), was calculated as follows:

$$\frac{g_b}{\rho_s[g(SG-1)d_{50}^3]^{1/2}} = \begin{cases} 4.6 \times 10^7(\tau^*)^8 & \tau^* < 0.065 \\ \frac{8.5(\tau^*)^{1.8}}{[1+5.95\times10^{-6}(\tau^*)^{-4.7}]^{1.43}} & \tau^* > 0.065 \end{cases} \tag{4}$$

The time series data for the SMOGC experiments were used to perform a sediment mass balance for the CV shown in Fig. 2, partition the amount of sand forming the sand ridge and sand patches upstream and within the clast array region, respectively, and the amount of sand trapped in the interstices of the porous bed. the mass balance was not performed for the SMOG experiments, because no bed features were prevalent. For the mass balance analysis, the bed-load rate, g_b, in Eq. (4) was converted to a volumetric rate (in m^3/s/m), defined as $q_b = g_b/\rho_s$ or $Q_b = bg_b/\rho_s$ where b is the flume width.

Mass Balance Analysis of Sediment

The analysis in the previous section was complemented with a mass balance analysis for the CV defined in Fig. 2. The mass of the incoming sand, M_{in}, was calculated as

$$(M_{\text{in}})_{CV} = \rho_s\left(\int_{t_{\text{initial}}}^{t_{\text{final}}} dV_{\text{in}}\right)_{CV} \tag{5}$$

where V_{in} = volume of the eroding sand over the sand bed section in m^3, corresponding to the 2.6 m section upstream of the CV, as shown in Fig. 2, where primarily erosion occurred; and t_{initial} and t_{final} = starting and ending time of the experiment (shown in Fig. 6), respectively. The portion of the incoming sand depositing within the CV, referred as "sand losses," M_{losses}, was determined as

$$\begin{aligned}(M_{\text{losses}})_{CV} &= (M_{\text{patches}} + M_{\text{ridge}} + M_{\text{infiltration}})_{CV} \\ &= \rho_s\left[\int_{t_{\text{initial}}}^{t_{\text{constant}}}(dV_{\text{patches}} + dV_{\text{ridge}} + dV_{\text{infiltration}})\right]_{CV}\end{aligned} \tag{6}$$

where t_{constant} = time when the bed-load rate entering the trap becomes pseudoconstant (Fig. 6), and the volumes of the formed bed features remain unchanged with time; M_{patches} and V_{patches} = mass and volume, respectively, of the deposited sand forming the sand patches around the clasts; M_{ridge} and V_{ridge} = mass and volume, respectively, of the accumulated sand forming the sand ridge; and $M_{\text{infiltration}}$ and $V_{\text{infiltration}}$ = mass and volume, respectively, of the infiltrated sand within the porous glass bead bed (Fig. 8). The amount of sand exiting the CV with time, M_{exit}, is the sand collected in the trap after t_{constant} (i.e., the approximate time when sand particles reached the trap) and is expressed as

$$(M_{\text{exit}})_{CV} = \rho_s\left(\int_{t_{\text{constant}}}^{t_{\text{final}}} Q_b dt\right)_{CV} \tag{7}$$

where Q_b = bed-load rate entering the sediment trap. The mass balance equation among the incoming, exiting, and depositing sand, written as

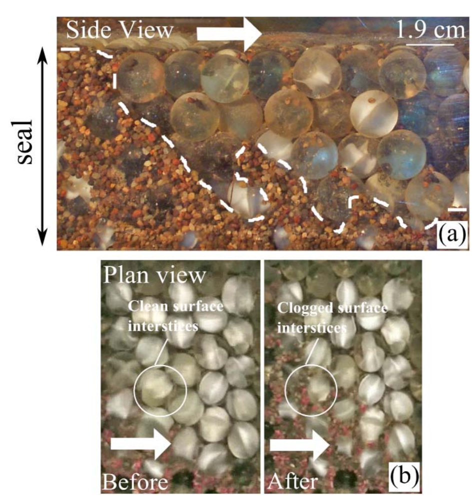

Fig. 8. Flume showing sediment infiltration within bed during SMOGC-1 experiment: (a) side view; (b) plan view; arrows indicate flow direction

J. Hydraul. Eng., 2011, 137(9): 871-883

Table 2. Mass Balance of Incoming, Exiting, and Depositing (Losses) Sand in CV

Experiment	$t_{constant}$ (h)	M_{in} (kg)	M_{losses} (kg)			M_{exit} (kg)	M_{in}-M_{losses}-M_{exit} (kg)
			Patches	Ridge	Infiltration		
SMOGC-1	580	60.75	6.44	38.22	10.65	4.94	~0
SMOGC-2	1.3	77.27	5.22	10.60	9.61	52.24	~0

$$(M_{in})_{CV} = (M_{losses})_{CV} + (M_{exit})_{CV} \quad (8)$$

was satisfied for both SMOGC experiments (see Table 2). On the basis of Table 2, for the SMOGC-1 (SMOGC-2) experiment, ~63% (~14%) of the eroded sand from the sand bed section deposited upstream of the clast array region forming the sand ridge, ~18% (~12%) infiltrated within the porous glass bead bed, ~11% (~7%) deposited upstream of the individual clasts forming the sand patches, and ~8% (~67%) exited the CV. A comparison of the amount of sand trapped within the CV (i.e., sand losses) between the SMOGC-1 (~92%) and SMOGC-2 (~33%) experiments suggests that the trapping efficiency of the clast array region reduces as the bed shear stress increases.

Flow Measurements around the Clasts

The purpose of the LSPIV measurements was to map the effects of clasts and bed morphological features on the free-surface flow velocity field within the clast array region and establish a correspondence between the flow field distribution and reported depositional patches. To do so, the distribution of the time-averaged resultant velocity, $\bar{V}$ (i.e., $\bar{V} = \sqrt{\bar{u}^2 + \bar{v}^2}$ where $\bar{u}$ and $\bar{v}$ are the time-averaged streamwise and transverse velocities, respectively), was compared for the SMOGC-1 experiment without and with the presence of the sand ridge and depositional patches. The measurements for the latter case (i.e., with the bed morphological features) were conducted when the sand ridge and sand patches upstream and within the clast array region obtained a mature shape. Seeding the flow with polystyrene foam material for the high bed shear stress conditions (i.e., the SMOGC-2 experiment) was challenging, and no repetitive flow measurements were collected. polystyrene foam particles agglomerated at the free-surface, making it challenging to measure accurately their displacement with time. As a result, the LSPIV measurements for the high applied bed shear stress condition are not reported in this paper.

A comparison of Figs. 9(a) and 9(b) for the SMOGC-1 experiment shows that higher velocities were recorded when the bed morphological features were present within the clast array region. The existence of the sand ridge upstream of the clast array region and the depositional patches within the region created flow constriction, leading to an ~70% increase in the overall streamwise flow velocity (i.e., the maximum velocity for SMOGC-1 without the presence of the bed morphological features was 0.13 m/s; the maximum velocity for the SMOGC-1 with the presence of the bed features was 0.22 m/s). A further comparison of Figs. 9(a) and 9(b) shows that the presence of patches increased the spatial variability in the magnitude of $\bar{V}$. For the case of the SMOGC-1 experiment with the bed morphological features present, fast moving fluid corridors were developed mostly between two adjacent rows of clasts in the streamwise direction. In this case, fast moving fluid areas were also developed in the stoss area of the clasts where the patches were present [Fig. 9(b)].

It was hypothesized that the flow field patterns shown in Fig. 9(b) reflect the local effects the depositional patches had on the free-surface flow field. In addition, the existence of the sand patches created local flow constriction, leading to an increase in the velocity magnitude of the approaching flow to the clasts. Therefore, it is not surprising that the flow patterns in Fig. 9(b) provide a striking correspondence with the chessboard geometry presented in Fig. 4(a), if indeed these patterns capturef the effects that this geometry haf on the free-surface flow.

To explain the reversal behavior in the location of the depositional patches around the clasts for the SMOGC-1 experiment, the magnitude of the vorticity vector, ω_z, was derived from the 2D velocity field ($\bar{u}$, $\bar{v}$) in the wake region of an arbitrary chosen clast as follows:

$$\omega_z = \left(\frac{\Delta \bar{v}}{\Delta x} - \frac{\Delta \bar{u}}{\Delta y}\right) \quad (9)$$

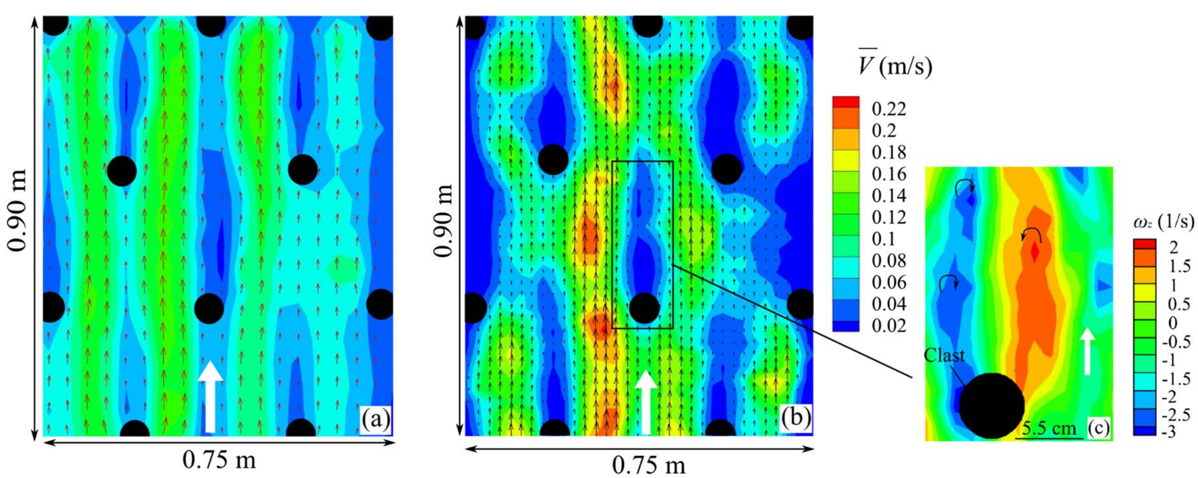

Fig. 9. Time-averaged resultant velocity $\bar{V}$ and its magnitude within the clast array region on the basis of the LSPIV results for SMOGC-1 without and with the presence of the sand patches around clasts, respectively: (a) velocity vectors; (b) isolines; (c) vorticity in the wake region [defined by the rectangular box in Fig. 9(b)] of an individual clast for SMOGC-1 experiment after formation of sand patches

J. Hydraul. Eng., 2011, 137(9): 871-883

Fig. 9(c) displays the vorticity representation and illustrates the existence of a Kármán vortex street, which is characterized by a repetitive pattern of clockwise and counterclockwise rotating swirling vortices in the wake region of the clast. Kármán streets are known to occur in partially submerged objects (e.g., Shamloo et al. 2001; Sadeque et al. 2008). The recirculation zone downstream of the clasts generates a backward flow in the wake that pushes the sand out and is assumed to be responsible for the absence of sand depositional patches behind the clasts. A similar backward flow pattern was observed by Shamloo et al. (2001) for flows with low relative submergences and was expected to be also present in the SMOGC-2 experiment.

Flow Resistance

Many studies have shown that sediment is transported only by the bed shear stress because of the grain roughness portion of the total bed shear stress, τ_t (e.g., Einstein and Barbarossa 1952; Engelund 1966; van Rijn 1984). Therefore, in this study, the total resistance to flow was decomposed into grain and form resistance to investigate the role of the clasts and bed morphological features on the bed-load rate for the CV defined in Fig. 2. The grain resistance, present in both the SMOGC and SMOG experiments, is induced by the bed skin roughness, whereas the form resistance, present only in the SMOGC experiments, is induced by the drag force of the clasts, sand ridge, and patches.

The total bed shear stress, τ_t, for the SMOGC experiments when the bed morphological features obtained their mature shape is expressed as

$$\tau_t = \tau_{\text{grain}} + \tau_{\text{clast}} + \tau_{\text{ridge}} + \tau_{\text{patches}} \tag{10}$$

where τ_{grain} = bed shear stress attributable to the grain roughness estimated as $\tau_{\text{grain}} = \rho g H S_{\text{constant}}$; and τ_{clast}, τ_{ridge}, τ_{patches} = added bed shear stress attributable to the clasts, sand ridge, and sand patches, respectively, each estimated from the following equation:

$$\tau_D = \frac{1}{2}\frac{A_p}{A_s} n \rho C_D U^2 \tag{11}$$

where n = number of elements (i.e., sand ridges, clasts, or patches) within a corresponding bed surface area, A_s; A_p = normal projection area of the element to the flow; U = approach velocity; and C_D = drag coefficient. The estimated values of n, A_s, A_p, U, and C_D for the clasts, the sand ridge, and sand patches for the SMOGC-1 experiment are summarized in Table 3 along with the corresponding bed shear stress, τ_D. The values for the drag coefficient, C_D, were obtained from well-documented values in the literature (e.g., White 1999) for different geometries such as spheres, 3D cones, and 2D wedges, which represent the shape of the clasts, sand patches, and sand ridge, respectively. Because of the absence of LSPIV data for the approach velocity in the vicinity of the clasts and sand patches for the SMOGC-2 experiment, no calculations are presented for this experiment.

Because the SMOGC-1 and SMOG-1 experiments were performed for nearly identical flow conditions (see Table 1), the total bed shear stress, τ_t, of 1.50 Pa obtained from Table 3 for the SMOGC-1 experiment was very close to the τ_t value of 1.55 Pa calculated for the SMOG-1 experiment on the basis of the τ^* value of 0.056 (see Table 1). However, for the SMOG-1 experiment, τ_t is equal to the bed shear stress attributable to the grain roughness, τ_{grain}, whereas for the SMOGC-1 experiment, τ_{grain} represented only 67% of τ_t. Therefore, although SMOGC-1 and SMOG-1 experiments were performed under similar τ_t, the difference in τ_{grain} between the two experiments, which is responsible for the movement of the sand particles, resulted in the difference between the bed-load rates. Because τ_{grain} for the SMOG-1 experiment was higher than the one for the SMOGC-1 experiment, the former experiment provided an ~20 times higher bed-load rate than the latter [see Figs. 6(a) and 7(a)]. Also, the bed-load rate for the SMOGC-1 experiment decreased with the growth of the bed features with time because of the increase of τ_{ridge} and τ_{patches} values and the decrease of τ_{grain}, while τ_t remained constant [Fig. 6(a)].

Table 3. Bed Shear Stress Partitioning for SMOGC-1 Experiment

Parameter	Grain	Clast	Ridge	Patches
n	—	40	1	37
C_D	—	0.4	1.2	0.3
U (m/s)	—	0.16	0.35	0.16
A_s (m^2)	—	4.5	2.75	4.5
A_p (m^2)	—	0.002375	0.0125	0.0018
τ_D (Pa)	1.00	0.11	0.33	0.06

Conclusions

This study presented unique experiments on the effects of an array of 40 clasts on the movement of sand over a gravel bed under low relative submergence conditions. The clasts were placed atop an immobile glass bead bed on a 2% packing density, corresponding to an isolated roughness regime. The effects of clasts on sand movement were examined, for the first time, not only within the clast array region, but also in the upstream section of the clast region. The experimental results revealed the formation of two bed morphological features new to the literature, namely, a sand ridge upstream of the clast array region and small depositional sand patches in the stoss of the individual clasts. The experimental work was complemented with a mass balance analysis to determine the percentage of the incoming sand that exited the CV and the percentage that was trapped within the CV, forming the unique bed morphological features. The added effects of the sand ridge and patches to the flow were investigated by performing LSPIV measurements around the clasts with and without the presence of the bed morphological features (i.e., SMOGC-1 with features versus SMOGC-1 without mature features). The primary findings of this research include the following:

1. The cause for the formation of the sand ridge was considered the increased resistance exerted by the clast array region to the flow, which created backwater effects upstream of the clast array region. Similarly, the formation of the depositional patches around the clasts was considered an outcome of the interaction between the flow and individual clasts.
2. The formation of the sand ridge and depositional patches led to the reduction of the incoming bed-load rate. By comparing the bed-load rates corresponding to different experiments, one can surmise that for relatively moderate bed shear stress conditions (i.e., ~$2.50\tau^*_{\text{cr}}$ where τ^*_{cr} is the critical bed shear stress), the collective presence of clasts and bed morphological features reduced the bed-load rate, on average, by a factor of ~20, whereas for higher bed shear stress conditions (i.e., ~$5.50\tau^*_{\text{cr}}$), by a factor of ~5.0.
3. Clast arrays with a packing density of 2% may not lead to significant depositional patches within the clast array region but can lead to the formation of a ubiquitous sand ridge upstream of the clast array region that should not be ignored because of its sizable geometry and significant effects on bed-load movement. A mass balance analysis performed within the test section for ~$2.50\tau^*_{\text{cr}}$ and ~$5.50\tau^*_{\text{cr}}$ illustrated that ~63% and 14%, respectively, of the incoming sand deposited upstream

J. Hydraul. Eng., 2011, 137(9): 871-883

of the clast array region forming the sand ridge. The amount of incoming sand forming the sand patches was ~11% and ~7% for the ~$2.50\tau^*_{cr}$ and ~$5.50\tau^*_{cr}$ conditions, respectively.

4. In the present study, the depositional patches formed in the stoss region of the clasts, whereas most of the available experimental studies (e.g., Brayshaw 1984; Strom et al. 2004) reported the accumulation of sediment in the wake region of the clasts. The reversal behavior in the location of the depositional patches around the clast has not been examined thoroughly in the literature because most of the available studies focused on the depositional patches under high relative submergence conditions in which the deposition of particles occurred in the wake area (e.g., Strom et al. 2004). It is suggested that for low relative submergences, the depositional patches were located in the stoss of the clasts because of backward flow and the presence of strong wake, and this hypothesis was tested further by performing flow measurements within the clast array region when the bed morphological features obtained a mature shape. Flow structures in the wake region of the individual clasts illustrated a vortex street and the creation of recirculation zone in the wake of the clasts. The recirculation zone generated a backward flow that was considered responsible for the absence of the sand depositional patches in the clast wake. A caveat to this finding were the flow measurements for the shallow experimental conditions limited to the free surface. In spite of this limitation, these results highlight the need for performing more detailed flow experiments capable of resolving mean local and turbulent flow quantities at scales comparable to the clasts.
5. The existence of the sand ridge and sand patches upstream and within the clast array region, respectively, created flow constriction, leading to an ~70% increase in the overall streamwise flow velocity within the clast array region for the SMOGC-1 experiment.
6. Comparisons of the flow resistance calculations for the SMOGC-1 and SMOG-1 experiments, with nearly identical flow conditions, showed that for SMOGC-1, the grain resistance represented only 67% of the total resistance, whereas for SMOG-1, the grain resistance was equal to the total resistance. This difference suggests that the bed-load rate for the SMOGC-1 experiment must be less in magnitude than the one for the SMOG-1 experiment, verified from the bed-load rate measurements. On the basis of this finding, it is evident that neglecting the form resistance of the clasts and the associated bed morphological features can introduce significant errors in bed-load predictions for gravel bed streams. It is not surprising, therefore, that most conventional sediment transport equations, which were developed for low gradient streams and do not account for the form roughness, tend to overestimate the amount of sediment transported by order of magnitudes in mountain streams (e.g., Rickenmann 1997; D'Agostino and Lenzi 1999).

The results of this study show that the effects of the sand ridge on the flow and incoming sediment are not negligible, for the 2% packing density, which may suggest that the location of engineered riffles sections and the selection of the clast packing arrangement should be made carefully, depending on the flow conditions and the goals of the stream restoration project.

Because of the complexity of the problem, some limitations exist for the reported findings of this experimental study. First, only the glass bead arrangement that corresponded to the most densely bed packing arrangement; that is, an average porosity of $n_p = 0.24$ (Allen 1982), was considered. The size of the porous structure of the glass bead bed will affect the amount of sand that infiltrates within the bed porous structure; that is, the higher the porosity, the larger the amount of sand that will infiltrate the interstices of the glass bead bed. Therefore, by performing experiments with a higher bed porosity, more sand will tend to infiltrate the bed structure, resulting in increased percentages of infiltrated sand, which may lead to the deviation from the reported results in this study. Nonetheless, the formation of the sand patches in the stoss region of the clasts was found to occur independently of the bed porosity (e.g., Carling 1984).

Another caveat of the experimental results presented in this paper relates to the use of a single packing density for the clasts. In this study, the 2% packing density was considered because it is commonly found in mountain streams. Clearly, the scenario examined for this paper will not replicate conditions of sand bed movement over gravel beds for a packing density of clasts corresponding to the wake interference (i.e., an ~30% packing density) or nearly skimming flow regime (i.e., an $\sim > 50\%$ packing density). For the latter cases, it is expected that the amount of deposited sediment within the clast region will increase (Papanicolaou and Kramer 2005; Yager et al. 2007). However, as Bunte and Poesen (1993) and others have shown, a critical packing density condition exists (i.e., ~20%) for trapping efficiency; when this condition is surpassed, the effectiveness of the clast array region to trap (or "harvest") more incoming sediment does not improve drastically. Which effects of clast packing density on the sand ridge formation and the evolution for packing densities greater than 2% remain inconclusive. The 2% packing density favors the formation of a sand ridge that has more pronounced geometric characteristics than the sand patches. Another factor which may affect the geometric characteristics of the sand ridge is the flume width. It is possible that a different flume width may result in a sand ridge with two or more depositional fronts. In this case, further investigation is needed to address the effects of flume width on the formation of the reported bed morphological features.

Acknowledgments

The authors would like to acknowledge the support provided by the NSF Hydroscience Division under NSF Grant No. EAR-0208358 and the support of The Paul C. and Sara Jane Benedict Fellowship for Study of Alluvial River Processes provided to the second author. The authors would also like to express their gratitude to the two anonymous reviewers for their excellent suggestions, which strengthened the paper.

Notation

The following symbols are used in this paper:

A = flow cross-sectional area;
A_p = normal projection area of the element to the flow;
A_s = bed surface area;
b = width of flume;
b/H = width to depth ratio;
C_D = drag coefficient;
CV = control volume;
d = glass bead diameter;
d_{50} = median sand particle diameter;
d_c = diameter of the clast;
F = Froude number;
g = gravitational acceleration;
g_b = bed-load rate by weight;
H = flow depth;

J. Hydraul. Eng., 2011, 137(9): 871-883

H_{cr} = critical flow depth for incipient motion;
H/d_c = relative submergence;
k = decay constant of the bed gradient;
M_{exit} = mass of exiting sand from the CV;
M_{in} = mass of incoming sand within the CV;
$M_{\text{infiltration}}$ = mass of sand infiltrating in the CV (porous glass bead bed);
M_{losses} = mass of total losses of sand within the CV;
M_{patches} = mass of depositing sand (sand patches) in the CV;
M_{ridge} = mass of depositing sand (sand ridge) in the CV;
n = number of elements;
n_p = average porosity;
Q = volumetric discharge;
Q_b = volumetric bed-load rate;
q_b = volumetric bed-load rate per unit width;
R_o = Rouse number;
R = Reynolds number;
S = gradient of the flume;
S_{constant} = bed slope after bed features obtained a mature shape;
S_{initial} = initial bed slope;
SG = specific gravity;
t = time;
t_{constant} = time when bed features obtained a mature shape;
t_{final} = ending time of the experiment;
t_{initial} = starting time of the experiment;
u_* = shear velocity;
U = approach velocity;
U_{bulk} = mean bulk velocity;
$u(t)$ = instantaneous free-surface x-longitudinal velocity;
$\bar{u}$ = time-averaged free surface x-longitudinal velocity;
$v(t)$ = instantaneous free-surface y-transverse velocity;
V_{in} = volume of incoming sand;
$V_{\text{infiltration}}$ = volume of infiltrating sand;
V_{patches} = volume of sand deposited forming the sand patches;
V_{ridge} = volume of sand deposited forming the sand ridge;
$\bar{v}$ = time-averaged free surface y-transverse velocity;
$\bar{V}$ = time-averaged resultant velocity;
x = longitudinal coordinate direction;
y = transverse coordinate direction;
z = vertical coordinate direction;
κ = von Kármán constant = 0.40;
ν = kinematic viscosity of water;
ρ = density of water;
ρ_s = density of sand;
σ_g = geometric standard deviation;
τ_{clast} = bed shear stress attributable to clasts;
τ_D = bed shear stress attributable to the different elements;
τ_{grain} = bed shear stress attributable to grain roughness;
τ_{patches} = bed shear stress attributable to sand patches;
τ_{ridge} = bed shear stress attributable to sand ridge;
τ_t = total bed shear stress;
τ^* = dimensionless bed shear stress;
τ^*_{cr} = dimensionless critical bed shear stress;
ω = fall velocity; and
ω_z = azimuthal vorticity.

References

Allen, J. R. L. (1982). “Sedimentary structures: Their character and physical basis.” *Developments in sedimentology*, Vol. 1, Elsevier, Amsterdam, Netherlands.

Benson, I. A., Valentine, E. M., Nalluri, C., and Bathurst, J. C. (2001). “Stabilizing the sediment bed in laboratory flumes.” *J. Hydraul. Res.*, 39(3), 279–282.

Boyer, C., and Roy, A. (1991). “Morphologie du lit autour d’un obstacle soumis à un écoulement en couche mince.” *Géographie physique et Quaternaire*, 45(1), 91–99 (in French).

Brayshaw, A. C. (1984). “Characteristics and origin of cluster bedforms in coarse-grained alluvial channels.” *Sedimentology of gravels and conglomerates*, Vol. 10, Canadian Society of Petroleum Geologists, Calgary, Alberta, Canada, 77–85.

Bunte, K., and Poesen, J. (1993). “Effects of rock fragment covers on erosion and transport of non-cohesive sediment by shallow overland flow.” *Water Resour. Res.*, 29(5), 1415–1424.

Carling, P. (1984). “Deposition of fine and coarse sand in an open-work gravel bed.” *Can. J. Fish. Aquat. Sci.*, 41(2), 263–270.

D’Agostino, V., and Lenzi, M. A. (1999). “Bedload transport in the instrumented catchment of the Rio Cordon—Part II: Analysis of the bedload rate.” *Catena*, 36(3), 191–204.

Dietrich, W. E. (1982). “Settling velocity of natural particles.” *Water Resour. Res.*, 18(6), 1615–1626.

Einstein, H. A., and Barbarossa, N. L. (1952). “River channel roughness.” Paper No. 2528, *Trans. Am. Soc. Civ. Eng.*, 117, 1121–1146.

Engelund, F. (1966). “Hydraulic resistance of alluvial streams.” *J. Hydraul. Div.*, 92(2), 315–326.

Fox, J. F., and Patrick, A. (2008). “Large-scale eddies measured with large scale particle image velocimetry.” *Flow Meas. Instrum.*, 19(5), 283–291.

Hauet, A., et al. (2008). “Experimental system for real-time discharge estimation using an image-based method.” *J. Hydrol. Eng.*, 13(2), 105–110.

Image J Version 1.37 [Computer software]. Wayne Rasband, Bethesda, MD.

Keshavarzy, A., and Ball, J. (1999). “An application of image processing in the study of sediment motion.” *J. Hydraul. Res.*, 37(4), 559–576.

Kim, Y. (2006). “Uncertainty analysis of non-intrusive measurement of river discharge using image velocimetry.” Ph.D. dissertation, Univ. of Iowa, Iowa City, IA.

Kleinhans, M. G., Wilbers, A. W. E., De Swaaf, A., and Van Den Berg, J. H. (2002). “Sediment supply-limited bedforms in sand-gravel bed rivers.” *J. Sediment. Res.*, 72(5), 629–640.

Meselhe, E. A., Peeva, T., and Muste, M. (2004). “Large scale particle image velocimetry for low velocity and shallow water flows.” *J. Hydraul. Eng.*, 130(9), 937–940.

Misri, R. L., Garde, R. J., and Ranga Raju, K. G. (1984). “Bed load transport of coarse non-uniform sediments.” *J. Hydraul. Eng.*, 110(3), 312–328.

Morris, H. M. (1955). “Flow in rough conditions.” Paper No. 2745, *Trans. Am. Soc. Civ. Eng.*, 120, 373–398.

Mueller, E. R., Pitlick, J., and Nelson, J. M. (2005). “Variation in the reference shields stress for the bed load transport in gravel-bed streams and rivers.” *Water Resour. Res.*, 41(4), W04006.

Muste, M., Xiong, Z., Schone, J., and Li, Z. (2004). “Validation and extension of image velocimetry capabilities for flow diagnostics in hydraulic modeling.” *J. Hydraul. Eng.*, 130(3), 175–185.

Papanicolaou, A. N., Diplas, P., Bala, M., and Dancey, C. L. (1999). “Computer vision technique for tracking bed load movement.” *J. Comput. Civ. Eng.*, 13(2), 71–79.

Papanicoalou, A. N., Diplas, P., Dancey, C. L., and Balakrishnan, M. (2001). “Surface roughness effects in near-bed turbulence: Implications to sediment entrainment.”*J. Eng. Mech.*, 127(3), 211–218.

Papanicolaou, A. N., Diplas, P., Evaggelopoulos, N., and Fotopoulos, S. (2002). “Stochastic incipient motion criterion for spheres under various bed packing conditions.”*J. Hydraul. Eng.*, 128(4), 369–380.

Papanicolaou, A. N., and Kramer, C. (2005). “The role of relative submergence on cluster microtopography and bedload predictions in mountain streams.” *Proc. Int. Symp. River, Coastal, and Estuarine Morphodynamics*, Taylor and Francis, London.

Parker, G. (2008). “Transport of gravel and sediment mixtures.” Chapter 3, *Sedimentation engineering: Processes, measurements, modeling, and practice*, Manual No. 110, M. Garcia, ed., ASCE, Reston, VA.

Polatel, C., Muste, M., Patel, V. C., Stoesser, T., and Rodi, W. (2005).

J. Hydraul. Eng., 2011, 137(9): 871-883

"Double-averaged velocity profile over large-scale roughness." *Proc., XXXI Congress*, Korea Water Resources Association, Seoul.
Rickenmann, D. (1997). "Sediment transport in Swiss torrents." *Earth Surf. Processes Landforms*, 22(10), 937–951.
Rickenmann, D. (2001). "Comparison of bed load transport in torrents and gravel bed streams." *Water Resour. Res.*, 37(12), 3295–3305.
Sadeque, M. A. F., Rajaratnam, N., and Loewen, M. R. (2008). "Flow around cylinders in open channels." *J. Eng. Mech.*, 134(1), 60–71.
Shamloo, H., Rajaratnam, N., and Katopodis, C. (2001). "Hydraulics of simple habitat structures." *J. Hydraul. Res.*, 39(4), 351–366.
Strom, K., and Papanicolaou, A. N. (2008). "Morphological characterization of cluster microforms." *Sedimentology*, 55(1), 137–153.
Strom, K., Papanicolaou, A. N., and Constantinescu, G. (2007). "Flow heterogeneity over 3D cluster microform: Laboratory and numerical investigation." *J. Hydraul. Eng.*, 133(3), 273–287.
Strom, K., Papanicolaou, A. N., Evangelopoulos, N., and Odeh, M. (2004). "Microforms in gravel bed rivers, formation, disintegration and effects on bedload transport." *J. Hydraul. Eng.*, 130(6), 554–567.
Tritico, H., and Hotchkiss, R. (2005). "Unobstructed and obstructed turbulent flow in gravel bed rivers." *J. Hydraul. Eng.*, 131(8), 635–645.
Tuijnder, A. P., Ribberink, J. S., and Hulscher, M. H. (2009). "An experimental study into the geometry of supply-limited dunes." *Sedimentology*, 56(6), 1713–1727.
Vallé, B., and Pasternack, G. B. (2006). "Field mapping and digital elevation modelling of submerged and unsubmerged hydraulic jump regions in a bedrock step-pool channel." *Earth Surf. Processes Landforms*, 31(6), 646–664.
van Rijn, L. C. (1984). "Sediment transport, Part III: Bed forms and alluvial roughness." *J. Hydraul. Eng.*, 110(12), 1733–1754.
White, F. M. (1999). *Fluid Mechanics*, 4th Ed., McGraw-Hill, New York.
Wohl, E. E. (2000). "Mountain rivers." *Water Resources*, Monograph 14, American Geophysical Union, Washington, DC.
Yager, E. M., Kirchner, J. W., and Dietrich, W. E. (2007). "Calculating bed load transport in steep boulder bed channels." *Water Resour. Res.*, 43(7), W07418.

J. Hydraul. Eng., 2011, 137(9): 871-883